β-decay feeding intensity distributions of ^{71,73}Ni

C. F. Persch,[1,*] P. A. DeYoung,[1,†] S. Lyons,[2,3,‡] A. Spyrou,[2,3,4] S. N. Liddick,[2,3,5] F. Naqvi,[2] B. P. Crider,[2,3] A. C. Dombos,[2,3,4] J. Gombas,[2,4] D. L. Bleuel,[6] B. A. Brown,[2,4,3] A. Couture,[7] L. Crespo Campo,[8] J. Engel,[9] M. Guttormsen,[8] A. C. Larsen,[8] R. Lewis,[2,5] S. Karampagia,[2,10] S. Mosby,[7] E. M. Ney,[9] A. Palmisano,[2,4,3] G. Perdikakis,[2,11,3] C. J. Prokop,[2,5] T. Renstrøm,[8] S. Siem,[8] M. K. Smith,[2,3] and S. J. Quinn[2,4,3]

[1]*Department of Physics, Hope College, Holland, Michigan 49422, USA*
[2]*National Superconducting Cyclotron Laboratory, Michigan State University, East Lansing, Michigan 48824, USA*
[3]*Joint Institute for Nuclear Astrophysics, Michigan State University, East Lansing, Michigan 48824, USA*
[4]*Department of Physics and Astronomy, Michigan State University, East Lansing, Michigan 48824, USA*
[5]*Department of Chemistry, Michigan State University, East Lansing, Michigan 48824, USA*
[6]*Lawrence Livermore National Laboratory, Livermore, California 94550-9234, USA*
[7]*Physics Division, Los Alamos National Laboratory, Los Alamos, New Mexico 87545, USA*
[8]*Department of Physics, University of Oslo, NO-0316 Oslo, Norway*
[9]*Department of Physics and Astronomy, University of North Carolina, Chapel Hill, North Carolina 27599, USA*
[10]*Grand Valley State University, Allendale, Michigan 49401, USA*
[11]*Central Michigan University, Mt. Pleasant, Michigan 48859, USA*

(Received 15 September 2020; accepted 7 April 2021; published 13 May 2021)

This paper presents the β-decay feeding intensity distribution and Gamow-Teller transition strength distribution of ^{71,73}Ni. These quantities were measured using the technique of total absorption spectroscopy at the National Superconducting Cyclotron Laboratory with the Summing NaI(Tl) detector. These measurements provide sensitive constraints to theoretical models used to predict β-decay properties far from stability for astrophysical applications. Specifically, for the astrophysical r process, the majority of the involved nuclei are not accessible by current facilities, and the nuclear input is mainly provided by theory. The present work reports on two neutron-rich nickel isotopes in the region where the weak r process is expected to be relevant in stellar nucleosynthesis. The experimental results are compared to two theoretical models, namely the shell model and the quasiparticle random-phase approximation, to help further refine theoretical calculations and aid in future r-process studies.

DOI: 10.1103/PhysRevC.103.055808

I. INTRODUCTION

The rapid neutron-capture process (r process) is a complex astrophysical process that is responsible for the synthesis of roughly half of the isotopes of elements above Fe [1]. It involves long chains of neutron-capture reactions and β decays, together with β-delayed neutron emissions, possibly fission, and often (γ, n) reactions on neutron-rich isotopes. This astrophysical process is expected to take place in extremely neutron-rich environments such as supernovae [2–5] and/or binary neutron-star mergers (NSM) [6,7]. The first observation of a kilonova light emission in 2017, in conjunction with gravitational waves from a NSM event [8] showed that NSMs are an important site for the r process. Recently, the first direct observation of a heavy element (strontium) in the aftermath of the NSM event confirmed the previous interpretation [9].

The r process, together with the slow neutron capture process (s process), have been considered the two main processes responsible for heavy-element nucleosynthesis, together with small contributions from the p process for proton-rich isotopes. However, recent studies have shown that these processes are not enough to explain all astronomical observations, especially for medium-heavy nuclei. Possible contributions from a weak r process [10], the νp process [11], the light element primary process [12], the intermediate neutron-capture process (i process) [13], and more are being investigated. In order to disentangle the contributions from the various possible processes, accurate nuclear physics input is needed.

Nuclear properties relevant to the r process include the half-lives of all participating nuclei, β-delayed neutron-emission probabilities, neutron-capture cross sections, nuclear masses, and fission properties [14,15]. All of these properties have an impact on calculated abundance distributions [16,17]. In the present work we focus on the study of β-decay properties. Not all relevant nuclei are accessible in current radioactive beam facilities, and therefore r-process models have to rely on theoretical calculations. β-decay properties

*cole.persch@colorado.edu
†deyoung@hope.edu
‡Current address: Pacific Northwest National Laboratory, Richland, Washington 99354, USA.

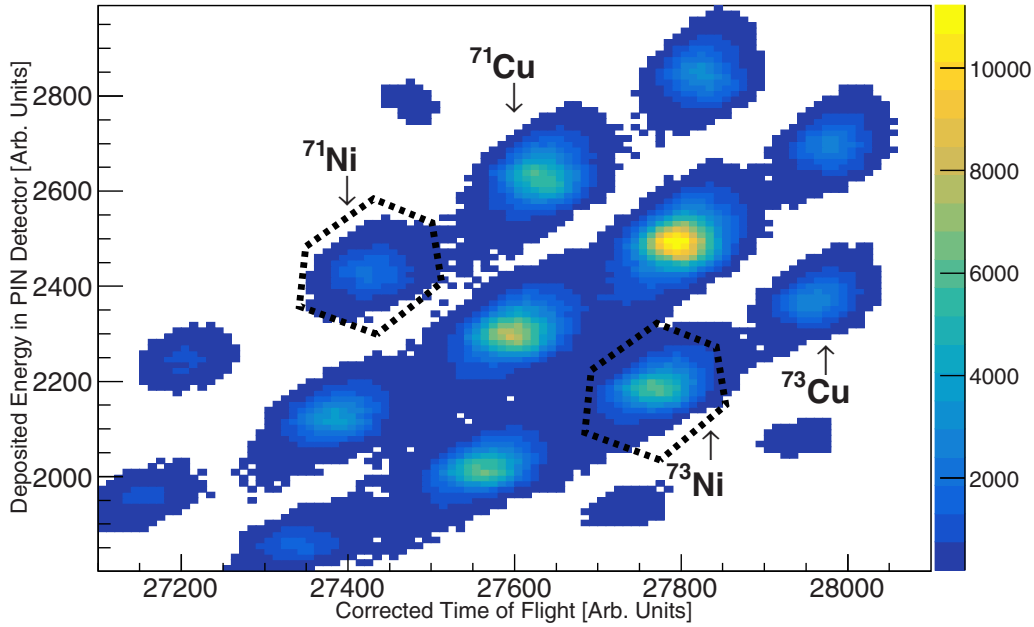

FIG. 1. A plot of the deposited energy versus ToF between two silicon PIN detectors. Each intense group corresponds to a different isotope in the beam. The two Ni isotopes studied in this work and the gates that define them are are shown. A small correction was applied to the ToF remove variations due to spread in the beam momentum. Channels with counts less than 0.02 of the full scale counts (yellow on-line) are not shown.

are typically calculated using quasiparticle random-phase approximation (QRPA) model [18–20]. These calculations are typically tested against known half-lives and β-delayed neutron emission probabilities. Both properties are "integral" quantities and depend on the β-decay feeding intensity, $I_\beta(E)$, and the Gamow-Teller strength distribution, B(GT). However, a more sensitive probe to test the validity of the theoretical calculations would be the direct comparison to experimental $I_\beta(E)$ and B(GT). In addition, comparing these quantities to shell-model calculations, as well as the QRPA, can also give insight into the nuclear structure of the nuclei of interest.

The present work focuses on the first extraction of $I_\beta(E)$ and B(GT) distributions of ^{71,73}Ni with total absorption spectroscopy (TAS). The experimental results are compared to corresponding shell-model and QRPA calculations. The TAS technique minimizes the Pandemonium effect [21], which was introduced more than 40 years ago. This term refers to difficulty in extracting $I_\beta(E)$ when low-efficiency detection systems are used, due to missing high-energy and/or low-intensity γ-ray transitions. Using a large volume, γ-ray calorimeter reduces the impact of the Pandemonium effect and provides more accurate $I_\beta(E)$ measurements. The TAS technique has been used extensively for $I_\beta(E)$ measurements by different groups around the world, e.g., Refs. [22–26].

The experimental details are presented in Sec. II, while the analysis techniques are described in Sec. III. Final results and comparison to theory are presented in Secs. IV and V and conclusions in Sec. VI.

II. EXPERIMENTAL DETAILS

The experiment took place at the National Superconducting Cyclotron Laboratory (NSCL) at Michigan State University. A ^{86}Kr primary beam at 140 MeV/nucleon impacted a ^{9}Be target, resulting in a secondary beam which passed through the A1900 fragment separator [27]. The separator was set to a 5% momentum acceptance, restricting the secondary beam to atomic numbers between 25 and 30 and mass numbers between 67 and 75. A thin, position-sensitive plastic scintillator at the separator was used as the start for time-of-flight (ToF) measurements. The specific A and Z of each implanted nucleus was determined on an event-by-event basis from the ToF and energy deposited in the first PIN detector. Figure 1 shows the groups corresponding to ^{71,73}Ni, the two-dimensional gates that defined each type of implant event, and other isotopes for orientation. The secondary beam was delivered to the experimental end station, after passing through two silicon PIN detectors. Both detectors were used for ToF and energy loss measurements. Each ion was implanted into a 1-mm-thick, position-sensitive, double-sided, silicon-strip detector (DSSD) [28,29]: a detector with 16 by 16 strips resulting in a total of 256 pixels. This allows each ion to be located with a resolution of 1.25 mm in two directions. The DSSD was used to detect high-energy implantation events (on the order of serval GeV) and their subsequent low-energy β-decay events (on the order of several MeV). A threshold of 120 keV was applied to the low-energy outputs. In order to distinguish a nucleus implant from a light particle passing through the DSSD, a silicon surface barrier detector was placed 25 mm downstream and acted as a veto detector.

The Summing NaI(Tl) detector (SuN) [30] surrounded the DSSD. SuN is a right-circular cylindrical detector that is 16 inches in diameter and length, with a 1.8-inch diameter borehole. This detector is segmented into eight optically isolated NaI(Tl) crystals, each connected to three photomultiplier tubes. SuN was used to detect the γ rays resulting from the

deexcitation of the excited daughter nuclei. SuN has a full-energy peak efficiency of 85(2)% for a 661-keV γ ray from a ^{137}Cs source [30]. Signals from all detectors were recorded using the NSCL Digital Data Acquisition System [31]. Other results from this experiment and more detailed descriptions of the setup can be found in Refs. [22,23,32–35].

III. ANALYSIS

A. Particle identification

Since both implantation and β events were registered by the DSSD, different criteria were required to distinguish the two and ensure that only valid events were processed. In order for an event to be considered an implant, a signal must have registered in both silicon PIN detectors, both sides of the low-gain DSSD, and no signal registered in the veto detector. An event was classified as a β decay if there was no signal in the PIN detectors, no signal in either side of the low-gain DSSD, a signal from both sides of the high-gain DSSD, and no signal in the veto detector. The identity of each implanted ion was determined via energy loss and ToF measurements.

B. γ analysis

Due to the presence of multiple isotopes, it is necessary to correlate each β detection with an implant using space and time considerations. A forward-time correlation was done by matching every β-decay event to the preceding implant event in the same pixel. If there was another implant within 1 s of the correlated implant, the correlation was thrown out to avoid incorrect correlation. The difference in time between the correlated β-decay event and the implant event is referred to as decay time. In order to estimate the amount of incorrect correlations, the same process was carried out in reverse time order, resulting in a random β correlation. This process is referred to as β correlation to distinguish from the τ correlation described later. More information about this process can be found in Refs. [29,36,37].

The high geometrical efficiency of SuN allowed for a TAS analysis to be carried out. When summing the energy measured in each segment of SuN event by event, the TAS spectrum is created, which is sensitive to the excitation energy of the populated level in the daughter nucleus. A second spectrum, called sum-of-segments, shows the individual energy measurements from each of the eight segments of SuN and gives insight into the specific γ rays emitted during the deexcitation of the daughter nucleus. The third spectrum included in the present analysis is the multiplicity spectrum which records the number of segments in SuN that detected energy during each event.

γ-Ray spectra were created for the two isotopes of interest, ^{71,73}Ni, with additional decay-time gates aiming at reducing possible contributions from the decay of the daughter isotopes: ^{71,73}Cu. For ^{71}Ni, the experimental spectra were gated on decay times from 0 to 2.56(3) s, the half-life of ^{71}Ni as seen in Table I. The half-life of the daughter nucleus, ^{71}Cu is 19.4(16) s [41], and is expected to contribute approximately 4.7% to the observed decays within the decay-time gate. This percentage was estimated using the Bateman equations. Due to the short half-life of the daughter nucleus ^{73}Cu (4.2(3) s [42]), the ^{73}Ni spectra were gated on a range of decay times (0 to 0.5 s) that is less than one half-life (0.84 s). This restricts the contribution of ^{73}Cu for 4.3% which was also found using the Bateman equations.

TABLE I. Information about the analyzed nuclei. Half-lives were taken from Ref. [38], discrete levels from Ref. [39], and Q values from Ref. [40].

Parent	^{71}Ni	^{73}Ni
$T_{1/2}$ parent (s)	2.56(3)	0.84(3)
$T_{1/2}$ parent (s) present work	2.49(18)	0.81(8)
Daughter	^{71}Cu	^{73}Cu
$T_{1/2}$ daughter (s)	19.4(16)	4.2(3)
Maximum discrete level (MeV)	3.0	2.3
Q value (MeV)	7.3	8.8
DICEBOX range (MeV)	3.1 to 6.0	2.4 to 6.7

C. Half-life analysis

When using the β-correlation method as described in Sec. III B, since the correlation is taking place with a single implant, there is a slight bias toward shorter decay times. In addition, it is not possible to get the proper daughter contri-

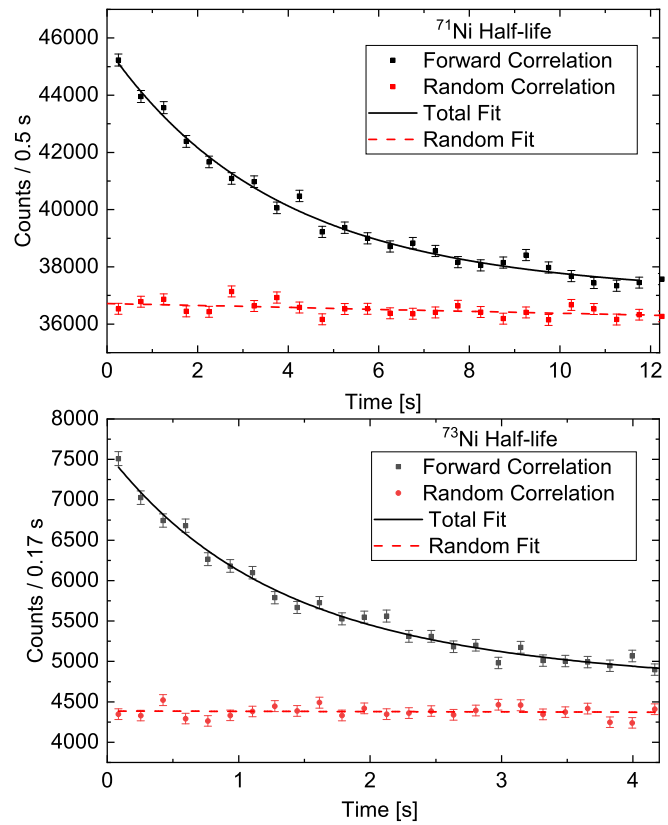

FIG. 2. Half-life measurements for ^{71,73}Ni. The random fits are included in the forward fits. Resulting measured half-lives are 2.49(18) s for ^{71}Ni and 0.81(8) s for ^{73}Ni. The ^{73}Ni fit has an additional component to account for the decay of ^{73}Cu.

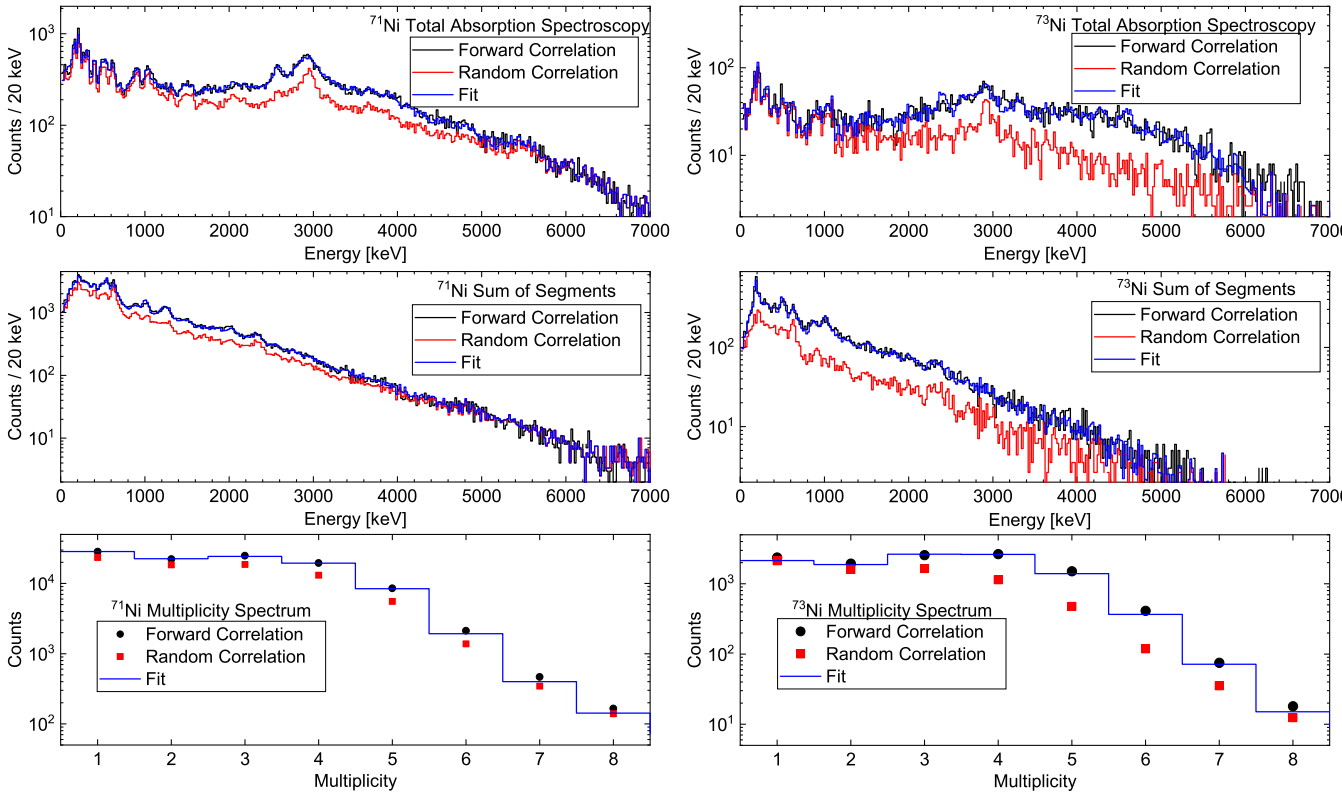

FIG. 3. The best fits of the data for the β decay of ^{71}Ni (left) and ^{73}Ni (right). The fit and data agree well and are difficult to distinguish in grayscale.

bution using the Bateman equations. For these reasons, the half-life estimate was done using the τ-correlation method, where each β event was correlated to every preceding implant within 20 s. The same method was used for the random τ correlation, but in the reverse time order. Note that the τ-correlation method is not well suited for γ-ray analysis due to the accumulation of significantly more random correlations compared to the β correlation. A histogram of the decay times using the forward and random correlations is shown in Fig. 2. The random decay curve was fit with a linear function, and the forward decay curve was then fit with an exponential function in addition to the linear fit of the random decay curve from 0 to 5 expected half-lives. Due to the short half-life of ^{73}Cu, an additional component was added to the fit of ^{73}Ni to account for the decay of the daughter. The resulting half-lives were 2.49(18) s for ^{71}Ni and 0.81(8) s for ^{73}Ni, both in agreement with the previously measured half-lives [38].

D. $I_\beta(E)$ extraction

With cascade information from the National Nuclear Data Center (NNDC), GEANT4 [43] was utilized to simulate the TAS, sum-of-segments, and multiplicity spectra for each level in the daughter nuclei [39]. GEANT4 accounts for the detection of γ rays, β particles, and the physical properties of both SuN and the DSSD. Since NNDC only lists energy levels of ^{71,73}Cu up to a certain excitation energy, it is necessary to simulate pseudolevels between the maximum level from the NNDC and the β-decay Q value. This was done with DICEBOX [44], a Monte Carlo simulation used to generate γ-ray cascades from given pseudolevels as described. The ranges used are shown in Table I, where the upper limits were set by the maximum energy observed in the TAS spectra.

A set of nine experimental spectra were created and fit with a sum of Monte Carlo spectra where the multiplicative coefficient associated with each daughter level was a free parameter. The experimental TAS, sum-of-segments, and multiplicity spectra, generated from β-correlated events, are shown in Fig. 3. (It proved impossible to use spectra from the τ-correlated events because $\approx$80% of the events in the forward correlation spectrum are due to random correlations.) To increase the sensitivity of the fitting procedure, six additional TAS-gated spectra were added. The sum-of-segments and multiplicity spectra were gated on different TAS regions. For ^{71}Ni these three TAS regions were 0.0–1.0 MeV, 1.0–3.0 MeV, and 3.0–7.5 MeV. For ^{73}Ni these three TAS regions were 0.0–1.5 MeV, 1.5–4.5 MeV, and 4.5–9.0 MeV. The nine experimental spectra together with the same nine spectra from GEANT4 for each simulated level were fed into a fitting program, and the coefficients were varied to minimize χ^2. Normalizing the sum of the resulting coefficients to 100% gave the $I_\beta(E)$ of each isotope. This process is described in more detail in Ref. [24].

Since some of the known levels listed on NNDC did not have a spin and parity assignment, these properties had to be assumed. To measure the impact of these assumptions, 10 additional sets of GEANT4 and DICEBOX spectra were generated for each isotope, with the level spins and parities

TABLE II. $I_\beta(E)$ for ^{71}Ni ground state. All intensity values below 10^{-3}% were omitted.

Energy (keV)	Intensity (%)	Error (±)
534.44	2.5	0.4
981.32	0.1	0.3
1895.16	0.1	0.4
2289.97	0.9	0.4
2551.5	8.3	1.3
2599.84	3.1	0.7
2805.9	10.0	1.6
2867.2	5.2	1.0
2925.21	3.1	0.9
3034.59	8.7	1.6
3100	5.1	1.3
3220	3.3	1.9
3260	1.8	2.8
3300	3.3	2.1
3460	6.7	1.3
3620	2.4	1.2
3700	4.5	1.2
3900	8.1	1.3
4100	5.7	1.0
4300	2.8	0.7
4500	2.2	0.9
4600	2.7	1.0
4800	2.4	0.9
4900	1.2	0.9
5300	2.7	1.2
5400	0.3	1.5
5600	1.9	0.9
6000	0.6	1.2

TABLE III. $I_\beta(E)$ for ^{73}Ni. All intensity values that were below 10^{-3}% are omitted.

Energy (keV)	Intensity (%)	Error (±)
166.07	0.6	0.3
2161.6	0.24	0.21
2386.0	9.8	1.0
2620	1.5	0.4
2660	4.9	0.8
2780	5.2	0.6
2840	4.4	0.6
2900	0.1	0.3
2990	3.8	0.4
3300	8.8	1.2
3500	0.18	0.25
3610	3.6	1.0
3865	6.3	1.2
4085	3.7	0.8
4275	10.1	1.3
4575	11.97	1.3
4875	5.9	1.0
5100	0.5	0.3
5175	5.4	0.7
5300	2.5	0.4
5400	0.01	0.5
5575	3.6	0.5
5800	2.21	0.2
6200	2.4	0.4
6380	0.61	0.26
6575	0.9	0.3
6880	1.0	0.4

randomized as ±1 from the original spin used and random parity. Fitting each of these sets produced the same coefficients within 1% of the values presented in Tables II and III, confirming that these assumptions had no significant impact within the measured uncertainty.

As mentioned earlier, the daughter of ^{73}Ni, ^{73}Cu, has a relatively short half-life. This resulted in some γ rays from ^{73}Zn appearing in the ^{73}Ni spectra, despite the gating on decay times less than 0.5 s. To account for this, additional TAS, sum-of-segments, and multiplicity spectra for discrete energy levels, as listed in ENSDF, from ^{73}Zn were included in the fit. The coefficients from ^{73}Zn were later removed, leaving just the ^{73}Cu level coefficients to be renormalized with respect to 100%. By summing the coefficients of the ^{73}Zn discrete levels, the contribution of ^{73}Zn γ rays was found to be less than 4%. A comparison of the two sets of simulated levels is shown in Fig. 4.

^{71}Ni has two β-decaying states: an isomer with a half-life of 2.3 s at 499 keV and the ground state with a half-life of 2.56 s [45]. The relative proportion of these two states produced in the fragmentation reaction is unknown. However, the excited isomeric state mainly populates the ground state and the 454.2-keV level in ^{71}Cu [46], while the ground state does not feed these levels. In this experiment, the 454.2-keV level of ^{71}Cu was only observed to be populated at a rate of 0.7(2)% of the total ^{71}Ni decays, and the ground state had much larger rate of population of 32(5)%. Due to the large difference in J^π of the ground state of ^{71}Cu $3/2^-$ and the J^π of the nonisomer of ^{71}Ni $9/2^+$, we expect that the ground-state population mainly comes from the isomer with a J^π of $1/2^-$. This indicates that approximately 33(5)% of the ^{71}Ni particles were in the isomeric state. Table II lists $I_\beta(E)$ only for the ^{71}Ni ground state. Because the half-life of the daughter, 19.4 s, is much longer than the half-life of the ^{71}Ni, 2.5 s, the contribution to the spectra from decays of daughter is insignificant. Levels in ^{71}Zn were not included in the simulation.

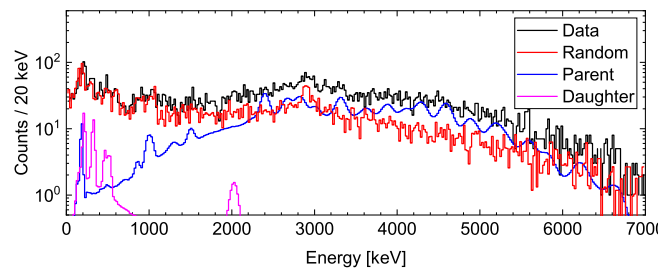

FIG. 4. Comparison of the TAS spectra from ^{73}Cu and ^{73}Zn. The curves associated with parent and daughter decays are from simulated spectra, while the data and random curves are from observation.

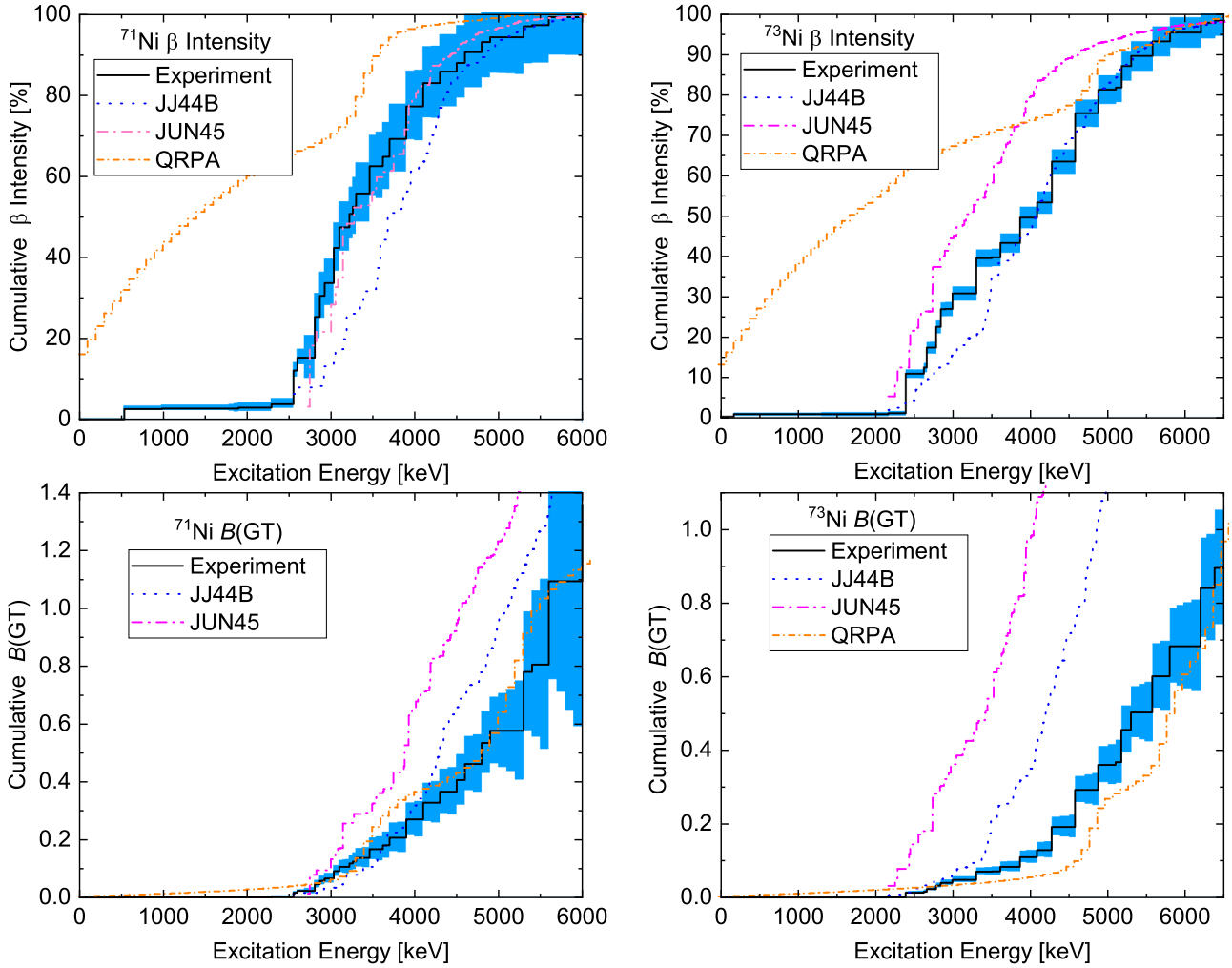

FIG. 5. The cumulative $I_\beta(E)$ and B(GT) for ^{71}Ni (left) and ^{73}Ni (right). The ^{71}Ni results are decays from the parent ground state to states in the daughter ^{71}Cu. Various shell-model and QRPA calculations are shown in the other dashed lines. The shaded region indicates experimental uncertainty determined by the χ^2 fitting. Both experimental B(GT) curves agree better with the QRPA calculations.

IV. RESULTS

The extracted $I_\beta(E)$ for the two isotopes of interest are presented in Tables II and III and in Fig. 5. In addition, the experimental $I_\beta(E)$ was used to calculate the Gamow-Teller strength distribution as follows:

$$B(\mathrm{GT}) = \frac{I_\beta(E)}{f(Q_\beta - E)T_{1/2}} K \left(\frac{g_V}{g_A}\right)^2, \qquad (1)$$

where $f(Q_\beta - E)$ is the Fermi integral, K is 6143.6(17) s [47], g_A/g_V is $-1.270(3)$ [48], and the half-lives where taken from Ref. [38]. The extracted B(GT)s are also shown in Fig. 5.

The experimental results are compared to two theoretical models, namely the shell model and QRPA which are described in the following subsections.

A. Shell-model calculations

The β-decay properties of ^{71,73}Ni were calculated with the NuShellX@MSU code [49] using two effective interaction Hamiltonians, JJ44B [50] and JUN45 [51], in the jj44 model space which is based on a ^{56}Ni core with the valence protons and neutrons occupying the $1f_{5/2}$, $2p_{1/2}$, $2p_{3/2}$, and $1g_{9/2}$ single-particle orbitals. For the B(GT) distribution, a quenching factor of 0.6 was used, smaller than the quenching factor of 0.77 used in the *sd* shell [52] and 0.74 for the *pf* shell [53]. In a previous publication, the β decay of ^{76}Ga [24] was studied, also in the jj44 model space and a quenching factor of 0.4 was used for the shell-model calculations. We chose the 0.6 quenching factor, as it seems to agree well with the experimental data both of the present study but also of a previous study of the β decay properties of ^{74,75}Cu [54]. The smaller quenching factor, compared to the values used for the *sd* and *pf* model spaces, is related to the fact that part of the Gamow-Teller strength lies outside of the model space. The appropriate value of the quenching factor for this model space remains to be studied and understood.

The shell-model calculations predict the ground-state spin and parity of ^{71}Ni to be $9/2^+$, in agreement with the experiment. The experimental half-life of the parent state is 2.56(3) s, and the half-life calculated using the JJ44B and JUN45 interactions is 2.34 s and 1.32 s, respectively, and can be

TABLE IV. A comparison of measure and modeled Ni half-lives for the ground and metastable states of ^{71}Ni.

$9/2^+$ $t_{1/2}$ (s)			$1/2^-$ $t_{1/2}$ (s)		
Expt.	JJ44B	JUN45	Expt.	JJ44B	JUN45
2.56(3)	2.34	1.32	2.3(3)	0.861	0.486

found in Table IV. Experimentally, a multiplet of low-lying, $9/2^+$, $7/2^+$, $1/2^-$, levels of ^{71}Ni has been observed, and it has been found that besides the ground state, the first $1/2^-$ state is also undergoing β decay, with a half-life of 2.3(3) s. The low energy spectrum of ^{71}Ni using the JJ44B and JUN45 Hamiltonians can be found in Table V and the calculated half-life of the β decay of $1/2^-$ using both Hamiltonians is tabulated in Table IV. For ^{73}Ni, both Hamiltonians predict the ground-state spin and parity to be the same as the experiment, $9/2^+$. The experimental half-life is 0.842(30) s, while the one predicted by the JJ44B and JUN45 Hamiltonians is 0.314 s and 0.164 s, respectively, also tabulated in Table VI. When the 0.4 quenching factor is used, the calculated half-lives become larger by a factor of 1.6/1.4, but still remain in disagreement with the experimental ones. More specifically, the half-life of ^{71}Ni with the JJ44B interaction is then overestimated and for the other cases the half-lives are still underestimated.

In the upper left panel of Fig. 5 the experimental cumulative β-decay feeding intensity of ^{71}Ni into the daughter nucleus ^{71}Cu is compared to shell-model and QRPA calculations. The lines labeled JJ44B and JUN45 refer to the β-decay feeding of the $9/2^+$ ground state of ^{71}Ni to ^{71}Cu. The $9/2^+$ ground state of ^{71}Ni decays to states of ^{71}Cu which are above 2.5 MeV. Looking at the cumulative β-decay feeding intensity of the $9/2^+$ state of ^{71}Ni in the daughter nucleus ^{71}Cu, the JUN45 Hamiltonian agrees very well with the experimental data, but for the same calculation, the JJ44B Hamiltonian underestimates the feeding. The cumulative feeding intensity of ^{73}Ni into ^{73}Cu, using the JUN45 Hamiltonian is overestimating the experimental data, while the JJ44B Hamiltonian agrees well with the experimental data. The calculated cumulative B(GT) curve of ^{71}Ni using the JJ44B Hamiltonian follows, overall, the experimental results, but the JUN45 Hamiltonian overestimates the experimental curve. For the ^{73}Ni nucleus, both interactions significantly overestimate the cumulative B(GT). The discrepancy for the JUN45 interaction begins from the lowest excitation energies and for the JJ44B interaction big discrepancies are noticed above $\approx$3.5 MeV. The calculated cumulative B(GT) curve depends strongly on the position of the first state of the daughter nucleus ^{73}Cu, which is fed by the β decay of ^{73}Ni. For example, shifting the first state of ^{73}Cu fed by ^{73}Ni from 2.16 to 2.46 MeV or 2.68 MeV, which is the value that a shell-model calculation using the JJ44B and JUN45 Hamiltonians give, will result in a shift of the cumulative B(GT) curve by 0.30 MeV and 0.50 MeV to the right, respectively. This rise of 14% and 24% respectively of the excitation energy reduces the discrepancy between the calculated and experimental cumulative B(GT) data and increases the calculated half-life by 35% and 57%.

TABLE V. A comparison of experimental and predicted ^{71}Ni low energy levels (MeV).

J^π	Expt.	JJ44B	JUN45
$\frac{9}{2}^+$	0.000	0.000	0.000
$\frac{7}{2}^+$	0.281	0.435	0.233
$\frac{1}{2}^-$	0.499	0.668	0.620

TABLE VI. A comparison of the experimental and predicted half-lives of ^{73}Ni.

$t_{1/2}$ (s)		
Expt.	JJ44B	JUN45
0.842(30)	0.314	0.258

To address the discrepancies between the calculated and experimental B(GT) results, the role of the single-particle energies was examined. The single-particle energies of JUN45 Hamiltonian were altered till the spectrum of ^{77}Ni and ^{79}Cu matched the spectrum derived from the solution of the Hartree-Fock equations using the SkX Skyrme interaction [55]. In Table VII, the $p_{3/2}$-$p_{1/2}$ spin-orbit splitting predicted by the two shell-model Hamiltonians and the SkX Skyrme interaction can be found. The cumulative B(GT) curve, calculated with the new single-particle energies, still had significant discrepancies from the experimental curve.

In summary, both Hamiltonians describe well the experimental cumulative $I_\beta(E)$, but overestimate the cumulative B(GT) of ^{71}Ni and ^{73}Ni. The shell-model calculations show a large fragmentation of the β-decay intensity. The calculated B(GT) values give stronger than expected contributions in the excited region mainly due to $\nu 2p_{1/2}$ to $\pi 2p_{3/2}$ transitions.

V. QRPA CALCULATIONS

In addition to testing shell-model calculations, we also compared our experimental β-decay properties with results from the QRPA. We employed the charge-changing Finite Amplitude Method [56,57] with a Skyrme functional to obtain the QRPA β-decay strength functions for axially deformed Hartree-Fock-Bogoliubov (HFB) ground states. Our calculations included allowed and first-forbidden contributions, and we treated the odd number of nucleons self-consistently in the equal filling approximation [58,59]. The single-particle space and functional were the same as those in Ref. [60], which used a single set of parameters to conduct a global calculation of β-decay rates in even-even isotopes. In particular, we used the Skyrme functional SKO′ for its ability to reproduce experimental β-decay Q values more consistently than

TABLE VII. Comparison of model calculations for the $p_{3/2}$-$p_{1/2}$ spin-orbit splitting (MeV).

	JJ44B	JUN45	SkX
^{77}Ni	1.06	1.42	1.35
^{79}Cu	1.83	1.83	1.27

similar functionals, and the time-odd and pairing couplings are the same as those from fit 1A in Ref. [60]. An effective axial-vector coupling of $g_A = 1$ was used during the fit and in all the calculations described below. The feeding intensity $I_\beta(E)$ is calculated as the cumulative integrated shape factor [56], normalized as a percentage of the total rate. To obtain strength as a function of the daughter excitation energy, we assumed that the lowest-energy transition in the strength functions is the ground-state to ground-state transition and shifted the strength so this transition lies at zero energy. All our calculated strength functions were folded with an artificial Lorentzian half-width of 0.1 MeV.

The HFB calculation for ^{71}Ni produced a slightly oblate $J^\pi = 9/2^+$ ground state with $\beta_2 = -0.020$. The artificial width in the strength function smooths out the $I_\beta(E)$ and, when weighted with phase space, contributes to the final rate. This contribution gives $I_\beta(E)$ artificially larger values at lower energies where the phase space is large. However, it is clear that the QRPA indicates significant feeding to daughter states around 3.5 MeV. The artificial width also smooths the cumulative Gamow-Teller strength, but it does not affect the total strength. We find fairly good agreement between the QRPA and experiment for the Gamow-Teller strength in ^{71}Ni. To get a sense of the contribution of the width to the rate, we also used contour integration to calculate the half-life [56,61], leading to the true QRPA result without any artificial contributions from the width. We calculated $T_{1/2} = 21$ s with this method, compared to 7 s from the integrated shape factor. From the contour integration results we also extracted the contribution of first-forbidden channels. We determined that ≈5% of the total rate comes from first-forbidden decay.

For ^{73}Ni, we calculated an HFB ground state with $J^\pi = 9/2^+$ and $\beta_2 = 0.001$. The width's artificial contribution to $I_\beta(E)$ is also evident here, but we can identify feeding to states at around 2.25 and 4.75 MeV. The QRPA slightly underpredicts the cumulative Gamow-Teller strength, unlike the shell model, but overall displays an adequate level of agreement with experiment. The half-life computed with contour integration is $T_{1/2} = 6.2$ s, while that computed from the integrated shape factor is 1.7 s, the disagreement once again mostly coming from the contribution of the artificial width at lower energies. The contour integration indicates 15% of the total rate is due to first-forbidden contributions.

VI. CONCLUSIONS

In an effort to improve the nuclear input for r-process calculations, the $I_\beta(E)$ of ^{71,73}Ni was measured for the first time using the technique of total absorption spectroscopy. The isotopes of interest were produced at the Coupled Cyclotron facility at Michigan State University and were implanted at the center of the SuN detector. The implanted ions were identified and correlated with subsequent β decays. The resulting experimental $I_\beta(E)$ and B(GT) distributions were then compared to shell-model and QRPA calculations to constrain these models. Similarly to other studies in this region, shell-model calculations are in reasonable agreement with the data. However, astrophysical calculations typically use QRPA calculations which are available at a more global scale than the shell model. Previous comparisons of QRPA calculations with experimental data were not able to reproduce the large fragmentation of $I_\beta(E)$ at higher energies. In the present work, QRPA is in excellent agreement with the experimental results at high energies and reproduces the large fragmentation of the strength. The agreement is not as good at low energies; however, due to the strong energy dependence of the B(GT) as a function of energy, the B(GT) is in excellent agreement with the experiment despite the low-energy discrepancy in the $I_\beta(E)$.

We plan to continue our investigation of β-decay properties in this mass region and also expand to higher masses which are also of major importance for the astrophysical r process.

ACKNOWLEDGMENTS

We gratefully acknowledge the support of NSCL operations staff. This work was funded in part by the National Science Foundation under Grants No. PHY-1613188, No. PHY 1102511 (NSCL), No. PHY 1913554, No. PHY 1811855, No. PHY 1430152 (Joint Institute for Nuclear Astrophysics), No. PHY 1350234 (CAREER), No. DUE-1153600, No. PHY-1306074, and No. DE-SC0018223 (SciDAC NUCLEI project). This material is based upon work supported by the U.S. Department of Energy, National Nuclear Security Administration through Grant No. DOE-DE-NA0003906 and under Award No. DE-NA0003180 (Nuclear Science and Security Consortium), and by the U.S. Department of Energy, Office of Science, Office of Nuclear Physics under Grant No. DE-SC0020451. Work performed under the auspices of Lawrence Livermore National Laboratory under Contract No. DE-AC52-07NA27344. A.C.L. gratefully acknowledges funding by the European Research Council through ERC-STG-2014 under Grant No. 637686, and support from the "ChETEC" COST Action (CA16117), supported by COST (European Cooperation in Science and Technology).

[1] M. Arnould, S. Goriely, and K. Takahashi, Phys. Rep. **450**, 97 (2007).
[2] S. E. Woosley, J. R. Wilson, G. J. Matthews, R. D. Hoffman, and B. S. Meyer, Astrophys. J. **433**, 229 (1994).
[3] L. Hüdepohl, B. Müller, H.-T. Janka, A. Marek, and G. G. Raffelt, Phys. Rev. Lett. **104**, 251101 (2010).
[4] T. Fischer, S. Whitehouse, A. Mezzacappa, F. K. Thielemann, and M. Liebendörfer, Astron. Astrophys. **517**, A80 (2010).
[5] G. Martínez-Pinedo, T. Fischer, A. Lohs, and L. Huther, Phys. Rev. Lett. **109**, 251104 (2012).
[6] S. Wanajo, Y. Sekiguchi, N. Nishimura, K. Kiuchi, K. Kyutoku, and M. Shibata, Astrophys. J. **789**, 39 (2014).
[7] O. Just, A. Bauswein, R. Pulpillo, S. Goriely, and H. T. Janka, Mon. Not. R. Astron. Soc. **448**, 541 (2015).
[8] D. Kasen, B. Metzger, J. Barnes, E. Quataert, and E. Ramirez-Ruiz, Nature **551**, 80-84 (2017).

[9] D. Watson, C. J. Hansen, J. Selsing, A. Koch, D. B. Malesani, A. C. Andersen, J. P. U. Fynbo, A. Arcones, A. Bauswein, S. Covino, A. Grado, K. E. Heintz, L. Hunt, C. Kouveliotou, G. Leloudas, A. J. Levan, P. Mazzali, and E. Pian, Nature **574**, 497 (2019).

[10] R. Surman, G. C. McLaughlin, M. Ruffert, H.-Th. Janka, and W. R. Hix, Astrophys. J. **679**, 117 (2008).

[11] C. Fröhlich, G. Martínez-Pinedo, M. Liebendörfer, F.-K. Thielemann, E. Bravo, W. R. Hix, K. Langanke, and N. T. Zinner, Phys. Rev. Lett. **96**, 142502 (2006).

[12] F. Montes, T. C. Beers, J. Cowan, T. Elliot, K. Farouqi, R. Gallino, M. Heil, K.-L. Kratz, B. Pfeiffer, M. Pignatari, and H. Schatz, Astrophys. J. **671**, 1685 (2007).

[13] J. J. Cowan and W. K. Rose, Astrophys. J. **212**, 149 (1977).

[14] C. J. Horowitz, A. Arcones, B. Côté, I. Dillmann, W. Nazarewicz, I. U. Roederer, H. Schatz, A. Aprahamian, D. Atanasov, and A. Bauswein, J. Phys. G **46**, 083001 (2019).

[15] A. Spyrou, Annals of Physics **412**, 168017 (2020).

[16] M. Mumpower, R. Surman, G. C. McLaughling, and A. Aprahamian, Prog. Part. Nucl. Phys. **86**, 86 (2016).

[17] D. Martin, A. Arcones, W. Nazarewicz, and E. Olsen, Phys. Rev. Lett. **116**, 121101 (2016).

[18] J. Krumlinde and P. Möller, Nucl. Phys. A **417**, 419 (1984).

[19] P. Möller, J. R. Nix, W. Myers, and W. Swiatecki, At. Data Nucl. Data Tables **59**, 185 (1995).

[20] P. Möller, J. R. Nix, and K.-L. Kratz, Nuclear Data and Nuclear Data Tables **66**, 131 (1997).

[21] J. C. Hardy, L. C. Carraz, B. Jonson, and P. G. Hansen, Phys. Lett. B **71**, 307 (1977).

[22] A. Spyrou, S. N. Liddick, F. Naqvi, B. P. Crider, A. C. Dombos, D. L. Bleuel, B. A. Brown, A. Couture, L. Crespo Campo, M. Guttormsen, A. C. Larsen, R. Lewis, P. Möller, S. Mosby, M. R. Mumpower, G. Perdikakis, C. J. Prokop, T. Renstrøm, S. Siem, S. J. Quinn, and S. Valenta, Phys. Rev. Lett. **117**, 142701 (2016).

[23] S. Lyons, A. Spyrou, S. N. Liddick, F. Naqvi, B. P. Crider, A. C. Dombos, D. L. Bleuel, B. A. Brown, A. Couture, L. C. Campo, J. Engel, M. Guttormsen, A. C. Larsen, R. Lewis, P. Möller, S. Mosby, M. R. Mumpower, E. M. Ney, A. Palmisano, G. Perdikakis, C. J. Prokop, T. Renstrøm, S. Siem, M. K. Smith, and S. J. Quinn, Phys. Rev. C **100**, 025806 (2019).

[24] A. C. Dombos, D.-L. Fang, A. Spyrou, S. J. Quinn, A. Simon, B. A. Brown, K. Cooper, A. E. Gehring, S. N. Liddick, D. J. Morrissey, F. Naqvi, C. S. Sumithrarachchi, and R. G. T. Zegers, Phys. Rev. C **93**, 064317 (2016).

[25] E. Nácher, A. Algora, B. Rubio, J. L. Taín, D. Cano-Ott, S. Courtin, Ph. Dessagne, F. Maréchal, Ch. Miehé, E. Poirier, M. J. G. Borge, D. Escrig, A. Jungclaus, P. Sarriguren, O. Tengblad, W. Gelletly, L. M. Fraile, and G. Le Scornet, Phys. Rev. Lett. **92**, 232501 (2004).

[26] A. Fijałkowska, M. Karny, K. P. Rykaczewski, B. C. Rasco, R. Grzywacz, C. J. Gross, M. Wolińska-Cichocka, K. C. Goetz, D. W. Stracener, W. Bielewski, R. Goans, J. H. Hamilton, J. W. Johnson, C. Jost, M. Madurga, K. Miernik, D. Miller, S. W. Padgett, S. V. Paulauskas, A. V. Ramayya, and E. F. Zganjar, Phys. Rev. Lett. **119**, 052503 (2017).

[27] D. J. Morrissey, B. M. Sherrill, M. Steiner, A. Stolz, and I. Widenhoever, Nucl. Instrum. Methods Phys. Res., Sect. B **789**, 90 (2003).

[28] J. I. Prisciandaro, A. C. Morton, and P. F. Mantica, Nucl. Instrum. Methods Phys. Res., Sect. A **505**, 140 (2003), proceedings of the tenth Symposium on Radiation Measurements and Applications.

[29] A. C. Dombos, A. Spyrou, F. Naqvi, S. J. Quinn, S. N. Liddick, A. Algora, T. Baumann, J. Brett, B. P. Crider, P. A. DeYoung, T. Ginter, J. Gombas, E. Kwan, S. Lyons, W.-J. Ong, A. Palmisano, J. Pereira, C. J. Prokop, D. P. Scriven, A. Simon, M. K. Smith, and C. S. Sumithrarachchi, Phys. Rev. C **99**, 015802 (2019).

[30] A. Simon, S. J. Quinn, A. Spyrou, A. Battaglia, I. Beskin, A. Best, B. Bucher, M. Couder, P. A. DeYoung, X. Fang, J. Görres, A. Kontos, Q. Li, S. N. Liddick, A. Long, S. Lyons, K. Padmanabhan, J. Peace, A. Roberts, D. Robertson, K. Smith, M. K. Smith, E. Stech, B. Stefanek, W. P. Tan, X. D. Tang, and M. Wiescher, Nucl. Instrum. Methods Phys. Res., Sect. A **703**, 16 (2013).

[31] C. J. Prokop, S. N. Liddick, B. L. Abromeit, A. T. Chemey, N. R. Larson, S. Suchyta, and J. R. Tompkins, Nucl. Instrum. Methods Phys. Res., Sect. A **741**, 163 (2014).

[32] R. Lewis, S. N. Liddick, A. C. Larsen, A. Spyrou, D. L. Bleuel, A. Couture, L. C. Campo, B. P. Crider, A. C. Dombos, M. Guttormsen, S. Mosby, F. Naqvi, G. Perdikakis, C. J. Prokop, S. J. Quinn, T. Renstrøm, and S. Siem, Phys. Rev. C **99**, 034601 (2019).

[33] A. C. Larsen, J. E. Midtbø, M. Guttormsen, T. Renstrøm, S. N. Liddick, A. Spyrou, S. Karampagia, B. A. Brown, O. Achakovskiy, S. Kamerdzhiev, D. L. Bleuel, A. Couture, L. C. Campo, B. P. Crider, A. C. Dombos, R. Lewis, S. Mosby, F. Naqvi, G. Perdikakis, C. J. Prokop, S. J. Quinn, and S. Siem, Phys. Rev. C **97**, 054329 (2018).

[34] S. N. Liddick, A. Spyrou, B. P. Crider, F. Naqvi, A. C. Larsen, M. Guttormsen, M. Mumpower, R. Surman, G. Perdikakis, D. L. Bleuel, A. Couture, L. Crespo Campo, A. C. Dombos, R. Lewis, S. Mosby, S. Nikas, C. J. Prokop, T. Renstrøm, B. Rubio, S. Siem, and S. J. Quinn, Phys. Rev. Lett. **116**, 242502 (2016).

[35] A. Spyrou, A. C. Larsen, S. N. Liddick, F. Naqvi, B. P. Crider, A. C. Dombos, M. Guttormsen, D. L. Bleuel, A. Couture, L. Crespo Campo, J. Phys. G: Nucl. Part. Phys. **44**, 044002 (2017).

[36] A. I. Morales, J. Benlliure, M. Górska, H. Grawe, S. Verma, P. H. Regan, Zs. Podolyák, S. Pietri, R. Kumar, E. Casarejos, A. Algora, N. Alkhomashi, H. Álvarez-Pol, G. Benzoni, A. Blazhev, P. Boutachkov, A. M. Bruce, L. S. Cáceres, I. J. Cullen, A. M. Denis Bacelar, P. Doornenbal, M. E. Estévez-Aguado, G. Farrelly, Y. Fujita, A. B. Garnsworthy, W. Gelletly, J. Gerl, J. Grebosz, R. Hoischen, I. Kojouharov, N. Kurz, S. Lalkovski, Z. Liu, C. Mihai, F. Molina, D. Mücher, W. Prokopowicz, B. Rubio, H. Schaffner, S. J. Steer, A. Tamii, S. Tashenov, J. J. Valiente-Dobón, P. M. Walker, H. J. Wollersheim, and P. J. Woods, Phys. Rev. C **88**, 014319 (2013).

[37] T. Kurtukian-Nieto, L. Benlliure, and K.-H. Schmidt, Nucl. Instrum. Methods Phys. Res., Sect. A **589**, 472 (2008).

[38] S. Franchoo, M. Huyse, K. Kruglov, Y. Kudryavtsev, W. F. Mueller, R. Raabe, I. Reusen, P. Van Duppen, J. Van Roosbroeck, L. Vermeeren, A. Wöhr, K.-L. Kratz, B. Pfeiffer, and W. B. Walters, Phys. Rev. Lett. **81**, 3100 (1998).

[39] S. Franchoo, M. Huyse, K. Kruglov, Y. Kudryavtsev, W. F. Mueller, R. Raabe, I. Reusen, P. Van Duppen, J. Van Roosbroeck, L. Vermeeren, A. Wöhr, H. Grawe, K. L. Kratz, B. Pfeiffer, and W. B. Walters, Phys. Rev. C **64**, 054308 (2001).

[40] G. Audi, O. Bersillon, J. Blachot, and A. Wapstra, Nucl. Phys. A **624**, 1 (1997).
[41] E. Runte, W.-D. Schmiedt-Ott, P. Tidemand-Petersson, R. Kirchner, O. Klepper, W. Kurcewicz, E. Roeckl, N. Kaffrell, P. Peuser, K. Rykaczewski, M. Bernas, P. Dessagne, and M. Langevin, Nucl. Phys. A **399**, 1 (1983).
[42] M. Huhta, P. F. Mantica, D. W. Anthony, P. A. Lofy, J. I. Prisciandaro, R. M. Ronningen, M. Steiner, and W. B. Walters, Phys. Rev. C **58**, 3187 (1998).
[43] J. Allison *et al.*, Nucl. Instrum. Methods Phys. Res., Sect. A **835**, 186 (2016)
[44] F. Bečvář, Nucl. Instrum. Methods Phys. Res., Sect. A **417**, 434 (1998).
[45] K. Abusaleem and B. Singh, Nuclear Data Sheets **112**, 133 (2011).
[46] I. Stefanescu, D. Pauwels, N. Bree, T. E. Cocolios, J. Diriken. S. Franchoo, M. Huyse, O. Ivanov, Y. Kudryavtsev, N. Patronis, J. Van De Walle, P. Van Duppen, and W. B. Walters, Phys. Rev. C **79**, 044325 (2009).
[47] J. C. Hardy and I. S. Towner, Nucl. Phys. News **16**, 11 (2006).
[48] J. C. Hardy and I. S. Towner, Phys. Rev. C **79**, 055502 (2009).
[49] B. A. Brown and W. D. M. Rae, Nucl. Data Sheets **120**, 115 (2014).
[50] S. Mukhopadhyay, B. P. Crider, B. A. Brown, S. F. Ashley, A. Chakraborty, A. Kumar, M. T. McEllistrem, E. E. Peters, F. M. Prados-Estevez, and S. W. Yates, Phys. Rev. C **95**, 014327 (2017).
[51] M. Honma, T. Otsuka, T. Mizusaki and M. Hjorth-Jensen, Phys. Rev. C **80**, 064323 (2009).
[52] B. H. Wildenthal, M. S. Curtin, and B. A. Brown, Phys. Rev. C **28**, 1343 (1983).
[53] G. Martínez-Pinedo, A. Poves, E. Caurier, and A. P. Zuker, Phys. Rev. C **53**, R2602 (1996).
[54] F. Naqvi, S. Karampagia, A. Spyrou, S. N. Liddick, A. C. Dombos, D. L. Bleuel, B. A. Brown, L. Crespo Campo, A. Couture, B. Crider, T. Ginter, M. Guttormsen, A. C. Larsen, R. Lewis, P. Möller, S. Mosby, G. Perdikakis, C. Prokop, T. Renstrøm, and S. Siem (unpublished).
[55] B. A. Brown, Phys. Rev. C **58**, 220 (1998).
[56] M. T. Mustonen, T. Shafer, Z. Zenginerler, and J. Engel, Phys. Rev. C **90**, 024308 (2014).
[57] P. Avogadro and T. Nakatsukasa, Phys. Rev. C **84**, 014314 (2011).
[58] T. Shafer, J. Engel, and C. Fröhlich, G. C. McLaughlin, M. Mumpower, and R. Surman, Phys. Rev. C **94**, 055802 (2016).
[59] S. Perez-Martin and L. M. Robledo, Phys. Rev. C **78**, 014304 (2008).
[60] M. T. Mustonen and J. Engel, Phys. Rev. C **93**, 014304 (2016).
[61] N. Hinohara, M. Kortelainen, and W. Nazarewicz, Phys. Rev. C **87**, 064309 (2013).